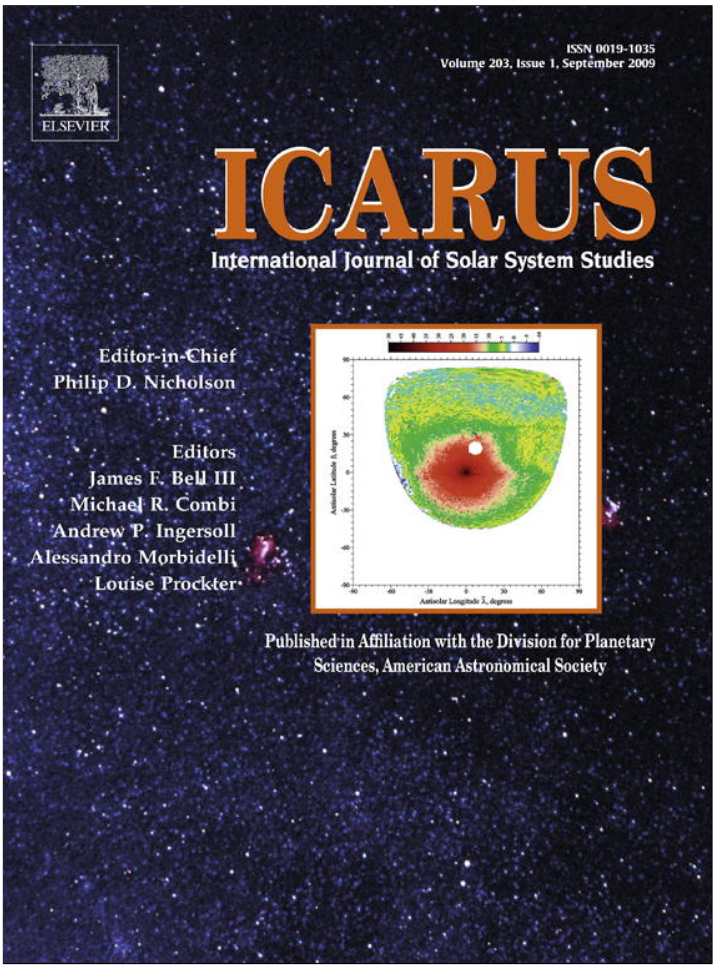

Icarus 203 (2009) 38–46

Contents lists available at ScienceDirect

Icarus

journal homepage: www.elsevier.com/locate/icarus

Mars magnetic field: Sources and models for a quarter of the southern hemisphere

Donna M. Jurdy *, Michael Stefanick

Department of Earth & Planetary Sciences, Northwestern University, 1850 Campus Drive, Evanston, IL 60208-2150, USA

ARTICLE INFO

Article history:
Received 13 July 2007
Revised 21 April 2009
Accepted 24 April 2009
Available online 22 May 2009

Keywords:
Mars, Surface
Magnetic fields
Cratering
Tectonics

ABSTRACT

The heavily-cratered southern hemisphere of Mars encompasses the planet's strongest, most widespread magnetization. Our study concentrates on this magnetized region in the southern hemisphere within 40° of latitude 40°S, longitude 180°W. First we rotate the coordinates to position the center at −40°, 180° and treat these new latitudes and longitudes as if they were Cartesian coordinates. Then, using an ordinary two-dimensional Fourier analysis for downward continuation, the MGS (MAG/ER) magnetic field data at satellite mapping elevation of ~400 km are extrapolated to 100 km, sources are estimated and used to model the fields. Quantitative comparison of the downward continued field with the aerobraking field for bins having angular deviation within ±30° gives correlation of .947, .868, and .769 for the B_r, B_θ and B_ϕ components, respectively. This agreement of the fields may result from most of the power in the magnetization resting in wavelengths ~400 km, with comparatively little at ~100 km. Over this region, covering nearly an octant of the planet, just a dozen sources can account for 94% of the variance of the magnetic field at the surface. In these models for the field an obvious asymmetry in polarity exists, with majority of the sources being positive. The locations of strongest surface magnetization appear to be near – but not actually within – ancient multi-ringed basins. We test the likelihood of this association by comparing the observed sources found within and near basins for two alternative basin location scenarios with random distributions. For both alternatives we find the observed distributions to be low-probability occurrences. If contemporaneous, this would establish that Mars' magnetic field extended to the time of impacts causing these basins.

1. Introduction

1.1. Background

Currently Mars does not have a magnetic field, therefore its remanent magnetism must be a relict of an earlier planetary field. The intensity of Mars' remanent magnetization reaching ~10 times that observed for the Earth requires both very strongly magnetic rocks and magnetization through a large section of the crust, possibly to a depth of 30 km (Connerney et al., 1999). Magnetic disruption near large impact craters such as Hellas and Argyre establishes that magnetization came before the impacts (Acuna et al., 1999; Nimmo and Gilmore, 2001) in the Mars' Noachian epoch ~4 Ga. Pressure-induced magnetic transition in pyrrhotite could demagnetize the Martian crust for large impacts (Rochette et al., 2003). Mitchell et al. (2007) observe that unlike Hellas and Argyre, magnetic sources circle Utopia just outside its topographic rim. They consider the alternatives that either Utopia demagnetized an already magnetized region, or that the sources represent magnetization of Utopia's inner ring at the instant of impact. The latter they note would establish the field as existing at the time of the Utopian impact.

How did Mars' crust become magnetized? Sleep (1994) first proposed Martian plate tectonics, with spreading ridges and subduction zones undergoing reorganization, but located in the northern hemisphere – where only patchy magnetized regions were later identified. The MGS magnetic mapping was initially interpreted in terms of lineations with reversals (Connerney et al., 1999) on Mars. More recently, from offsets of the magnetic field pattern in the Terra Meridiani region, Connerney et al. (2005) have identified offsets which they attribute to transform faults; based on the symmetry around an inferred ridge and the coherence of the magnetic profiles, they argued for magnetic reversals and crustal spreading analogous to Earth's seafloor spreading (Connerney et al., 2005). However, other interpretations of the magnetization are possible. Cain et al. (2003) constructed a 90-degree and order global spherical harmonic model of the scalar potential, cautioning that choices for contouring and color strongly influence visual appearance and interpretation of magnetic patterns. In a global fit of the low-elevation, aerobraking data with a 50-degree spherical harmonic analysis, downward continued to the surface, the strong magnetization in the southern hemisphere was interpreted with equi-dimensional sources rather than lineations (Arkani-

* Corresponding author. Fax: +1 847 491 8060.
E-mail address: donna@earth.northwestern.edu (D.M. Jurdy).

0019-1035/$ - see front matter © 2009 Elsevier Inc. All rights reserved.
doi:10.1016/j.icarus.2009.04.027

Hamed, 2001b). Also, our earlier models (Fig. 4, Jurdy and Stefanick, 2004) matched the scalar potential over nearly an eighth of the planet using just 14 vertical dipoles with intense magnetization. This model accounted for 64% of the variance; the resulting field matched the observed field at 100 km, with a correlation coefficient of 80%.

1.2. Motivation and dataset

Mars Global Surveyor (MGS) measured the most strongly magnetized crust in the heavily-cratered southern hemisphere of Mars. We believe that the analysis of the region with the most continuous, expansive, and intense magnetization offers the best opportunity for unraveling the mechanism and timing of magnetization, and the subsequent process of demagnetization. This could then lead to an improved understanding of the scattered patches of magnetized crust elsewhere on Mars. Thus, concentrating study on this strongly magnetized region, we analyze the magnetic patterns centered near 40°S, 180°, ranging ±40°, using a rotated Cartesian coordinate system.

Starting in 1999, the mapping phase of MGS followed the unexpected discovery of strongly magnetized crust that had been measured by the satellite at the elevation of ~100 km during its 1997 aerobraking phase (Acuna et al., 1999). We use data from this mapping phase, MAG/ER magnetic measurements at altitudes of 404 ± 30 km conveniently averaged, decimated, sorted and binned into 180 latitude and 360 longitude bins by degree, with estimates of each component in a spherical coordinate system with r (radial), ϕ (east–west), and θ (north–south) components (Connerney et al., 2001).

In our earlier paper (Jurdy and Stefanick, 2004) we extrapolated the MGS (MAG/ER) magnetic field components and constructed scalar potential from the mapping level down to the aerobraking level. Visual comparison of the downward continued field with the sparser, lower-elevation measurements suggested very good agreement. Here we quantitatively compare the fields to determine the correlation. Also, we seek to establish if the lower-elevation, pre-mapping data might contain additional information. Our ongoing investigation (Espley et al., 2007) of the North polar region, with more complete low elevation coverage, will facilitate direct comparison with the downward continued mapping field for development of the optimal algorithms for general use with Mars magnetic data.

Previously, we modeled the scalar potential for the magnetic field in the southern hemisphere region of interest (Jurdy and Stefanick, 2004). This paper continues our previous work, which we will refer to rather than duplicate definitions and arguments. Also, we include some technical points about our Fourier analysis and downward continuation not detailed in our earlier paper, which might be useful to others. Comparison of the field will be made to surface features, such as major faults and ringed basins – the sites of ancient impacts – to further constrain the time of magnetization.

2. Analysis

2.1. Co-ordinate transformation and Fourier analysis

The MGS magnetic data available had been gridded globally in spherical coordinates, as previously discussed. For our analysis we use the subset of data within ±40° of 40°S, 180°: at center latitude 40°S, longitudes range from 140° to 220°; at center longitude 180°, latitudes range from 0° to −80°. We then rotated coordinates with the center of our spherical coordinates located at 40°S, 180° in the original coordinates. This was done in such a way that our longitudes ranged from 140° to 220° and latitudes from −40° to +40°. Finally, we approximated, or pretended, that these coordinates could be treated as Cartesian coordinates. This allows the use of an ordinary two-dimensional Fourier analysis for downward continuation. The region studied, 40°S ± 40°, 180°W ± 40°, covers nearly an octant of Mars and encompasses the most strongly magnetized crust. Again, we emphasize that we use this approximation with the Cartesian variables, x, y, z rather than the usual spherical variables, ϕ, θ, r. Although the approximation neglects the curvature of the surface and may appear coarse, we argue that this provides an excellent representation of Mars' magnetic field over a limited area.

We have made our analysis using a rotated coordinate system, then restricted ourselves to a curved rectangle bounded by longitudes ±40° and then pretended that latitude and longitude were Cartesian coordinates. This simplified the problem, but serves only an approximation. How bad is the approximation and where is the error? One approach to assess the error is that we are approximating $\sin\theta$ to be $\simeq \theta$, where θ is the latitude as measured from the center of the rotated coordinate system (and so $\cos\theta \simeq 1$). Then the relative error as a function of latitude, θ, would be: $(\theta - \sin\theta)/\sin\theta \simeq \theta^2/6$. (The angles for latitude are of course in radians.) At the center, latitude of 0° the error is 0%, and at 20° the error is 2.05%, whereas at 40°, the periphery of the projection we use, the error reaches 8.55% This seems acceptable, as we would not focus upon effects ±40°, but rather re-rotate the coordinates to center upon the region of interest. Another way to consider the errors would be to begin at the center (0°,0°) and to move away in various directions and see how errors accumulate.

In our earlier analysis, we showed this Cartesian representation serves as a good approximation (Jurdy and Stefanick, 2004). Starting with the vertical component of the magnetic field, B_z, we constructed a unique scalar potential, V, and independently obtained B_x and B_y, the horizontal components of the field, from the derivatives of that scalar potential. These derived components matched the observed horizontal components (cf. Figs. 1 and 3; Jurdy and Stefanick, 2004). Besides testing our co-ordinate transformation, this independently confirmed the internal consistency of the MGS magnetic dataset. Had an error existed in any one of the magnetic field components, a consistent scalar potential with these properties could not be constructed. In addition, that the downward continuation of the MGS mapping-phase data at ~400 km very closely matched the independent measurements at ~100 km of the aerobraking phase (Fig. 2b, Jurdy and Stefanick, 2004) further demonstrated the validity and utility of the Cartesian approximation. We utilize this approximation again here to model the magnetic patterns in the Martian southern hemisphere.

Using Cartesian coordinates offers numerous advantages, foremost obviating the requirement of spherical harmonics for analysis. Interpreting longitudes and latitudes as Cartesian coordinates, we are able to use ordinary two-dimensional Fourier analysis for downward continuation. Another advantage of this coordinate system is the lack of distortion: the region mapped extends 40° in each direction about the center, ±40° of 40°S, 180°. The Mercator projection preserves shape, but it grossly exaggerates the size of high latitude objects – the Greenland versus Africa effect. Such high-latitude distortion would stretch equi-dimensional magnetic sources to appear more linear, resembling stripes.

Here, and in our earlier paper, we have assumed that the fields are all small near the boundaries and have continued them across the boundaries as mirror images (see, e.g. Dahlquist and Bjorck, 1997, Section 9.4). The Fourier series will converge more rapidly, and we can use pure sine series, which is much simpler to program in two dimensions (see, e.g. Press et al., 1992, pp. 508–515). This allows us to have one, instead of the four components required for a general Fourier spectrum. The Fourier series are summed

using a two dimensional Fejer window which nearly tapers from a value of 1 at zero wavenumbers to a value of zero at the cutoff wavenumbers ($k = 36$ in our case). This reduces the Gibbs' phenomenon which would result from abruptly truncating at the cut off wavenumber (see e.g. Carslaw, 1930, especially Chapter 7; Klein, 1925, pp. 190–200).

2.2. Downward extrapolation

Downward continuation or vertical extrapolation allows extrapolation of the magnetic field from MGS satellite mapping level at elevation ~400 km to the aerobraking level at elevation ~100 km and to Mars' surface as well as beneath. The vertical extrapolation assumes that the fields all obey Laplace's equation in three dimensions and also assumes that sources are below the planet's surface. The Fourier amplitude, $\widehat{B}_z(k)$, increases with extrapolation by an exponential factor and becomes

$$\widehat{B}_z(k)\exp(|k|z_0) \tag{1}$$

where $k = (k_x, k_y)$ is the wavenumber vector and $|k| = \sqrt{k_x^2 + k_y^2}$ the vertical distance of the extrapolation (Kanasewich, 1981, pp. 54–57).

The role of noise and its minimization must be carefully considered in downward continuation. When Fourier analyzed, the vertical component of the magnetic field, B_z, shows an exponential decrease in amplitude which would be expected from sources at or near the surface. As we extrapolate the field downward, the noise component quickly increases (Claerbout, 1976, pp. 66–88). Even for a modest extrapolation from 400 to 270 km shown in Fig. 1, we can see for the one-dimensional case at the 180° meridian that noise grows exponentially at higher wavenumbers. The amplification of the noise components and the minimum in the spectrum near $k = 25$–30 are evident. Thus, the Fourier components beyond $k = 25$ (wavelength 360 km) must be dropped. In our analysis we have used a simple truncation at $k = 25$. We found this to be effective (Fig. 1, Jurdy and Stefanick, 2003). Because a transition exists between wavenumbers 20 and 30, one might use signal and noise estimates to create a Wiener optimal filter (Press et al., 1992, pp. 539–542) which would make a gentle transition from signal to noise. However, we did not use an optimal filter. This will be part of our future investigations.

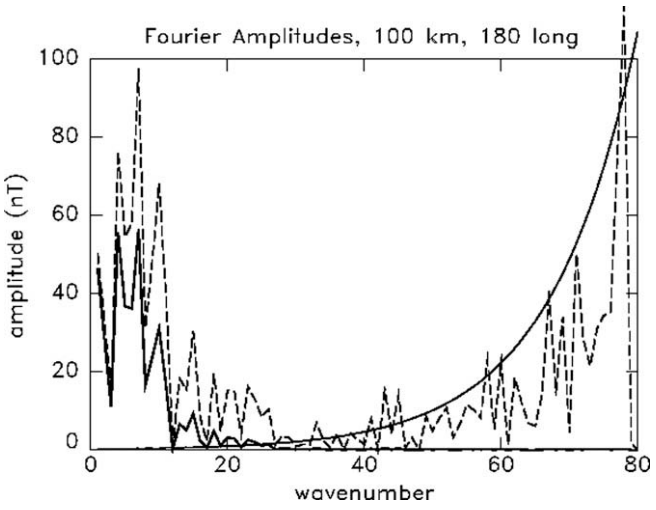

Fig. 1. The Fourier spectrum of the vertical component of the magnetic field, B_z, extending 40° along the 180° meridian (bold) and its downward extrapolation to about 270 km (dashed). This samples the strongest magnetization in Mars' southern hemisphere. The amplification of the noise components and the minimum in the spectrum near wavenumbers $k = 25$–30 are evident. The smooth curve shows a fit to white noise extrapolated downward. Thus to eliminate noise, in our analysis we truncated at wavenumber 25, corresponding to wavelength 360 km.

2.2.1. Comparison of MGS aerobraking and mapping-level data

Visual comparison of the downward-continued field with the more sparse aerobraking-level field (Acuna et al., 1999), though qualitative, suggested excellent agreement (Jurdy and Stefanick, 2004). In this section we present a quantitative comparison of the downward-continued data with the lower-level measurements made during the aerobraking phase. First, of particular interest, will be the comparison of the magnitudes of the downward continued field with the actual 100 km measurements. Second, of concern is whether locations of strongly magnetized regions for the downward continued field coincide with those of lower-level measurements. Also, here we take a "spy plane" approach to establish whether the satellite at aerobraking level might have detected any smaller patches of short-wavelength magnetization that would have eluded the higher-elevation mapping. However, the aerobraking data are noisy and also we are sampling at low resolution.

Though closer to the surface, Mars Global Surveyor's sparse aerobraking measurements contain significant noise. We used the dataset gridded into latitude and longitude boxes with elevations 80–190 km, 12 levels in all (Acuna et al., 1999). In processing this dataset, for each 2° box in the region within 40° of the point at latitude 40°S, longitude 180°W, all contributing measurements are used to form the magnitude of the magnetic vector, B:

$$|B| = \sqrt{B_r^2 + B_\theta^2 + B_\Phi^2} \tag{2}$$

The magnetic vectors jump around as we move from bin to bin, i.e. the field is noisy. For each grid point, p_0, we test the measurements by calculating the mean and standard deviation for points, p, within a $5^\circ \times 5^\circ$ grid surrounding (the resolution of our Fourier analysis). We then reject the point, p_0, if the ratio of the standard deviation, σ, to the mean μ, for n measurements exceeds a specified value. The mean is defined:

$$\mu = \frac{|\sum B(p)|}{n_p} \quad \text{for} \quad |p - p_0| \leqslant 2 \tag{3}$$

and the standard deviation determined for each component:

$$\sigma^2 = \frac{\sum |B(p) - B(p_o)|^2}{n_p} \tag{4}$$

The angle, α, between the mean and the standard deviation is:

$$\sin\alpha = \frac{\sigma}{\mu} \tag{5}$$

To minimize the noise we set some constraints. First, magnetic vectors were computed only for those grid points having five or more contributing measurements from the aerobraking data collected in 10 km altitude bins, from 80 to 190 km. Examining the individual aerobraking data values in $2^\circ \times 2^\circ$ bins, we find that in most cases the standard deviation exceeded the mean value, i.e. the individual magnetic vectors were pointing in "all" directions and were thus inconsistent. For this reason we restricted ourselves to the bins where the angular deviations were within ±30° of the mean. Thus, we require that $|B| \geqslant 50$ nt, and that the error $\leqslant 50\% B_L$, that is $\alpha \leqslant 30^\circ$, the difference between the vectors. Allowing $\alpha \leqslant 45^\circ$ would include vectors 90° apart which seems too large, so we have chosen 30°. These conditions to maximize the signal limit analysis to only 90 grid points with sufficient data coverage available and low enough noise to allow comparison in this 40° region.

Downward-continuation of the mapping-level field to 100 km provides a continuous representation there, spanning the few aerobraking passes available in the region of interest. We compare the

downward continued value of B_r, B_θ, B_Φ (Fig. 2a–c) versus the corresponding component of B_a, the aerobraking data, along with its associated standard deviation, σ. Correlation at the 90 grid points yields a correlation coefficient of .947. Coefficients for the B_θ and B_Φ components are .868 and .769, respectively, because of smaller signal and comparable or greater noise than B_r. The B_r component better reflects the surface magnetization because solar wind more strongly contaminates the B_θ and B_ϕ components (Nagy et al., 2004). Although increasing the required counts to 12 would yield an even higher correlation – reaching a coefficient of .970, this would then result in about half as many allowable grid points, only 45, for comparison. The very high correlation establishes that the magnitudes of the vector components of the downward continued field closely match the aerobraking measurements. Furthermore, the locations of strongly positive and negatives values match well. Here we note differences in the positive and negative polarities. In Fig. 2a, although there are about the same number of positive as negative points, the positive amplitudes of B_r are noticeably larger than the negative ones: one-quarter of the points have values less than −75 nT, whereas one-quarter of the positive values exceed 142 nT.

Does this data set culled from the full aerobraking set yield any additional information? The B_r aerobraking values for those grid points with errors and counts in required range do not hint at the existence of any strongly positive or negative spots not also evident on the downward continued set. Thus, for this region we have established that most of the power in the magnetization rests in wavelengths ∼400 km, and comparatively little at shorter wavelengths of ∼100 km.

We have performed a quantitative comparison of the downward continued, mapping level magnetic data with measurements made during the lower elevation aerobraking phase. This analysis

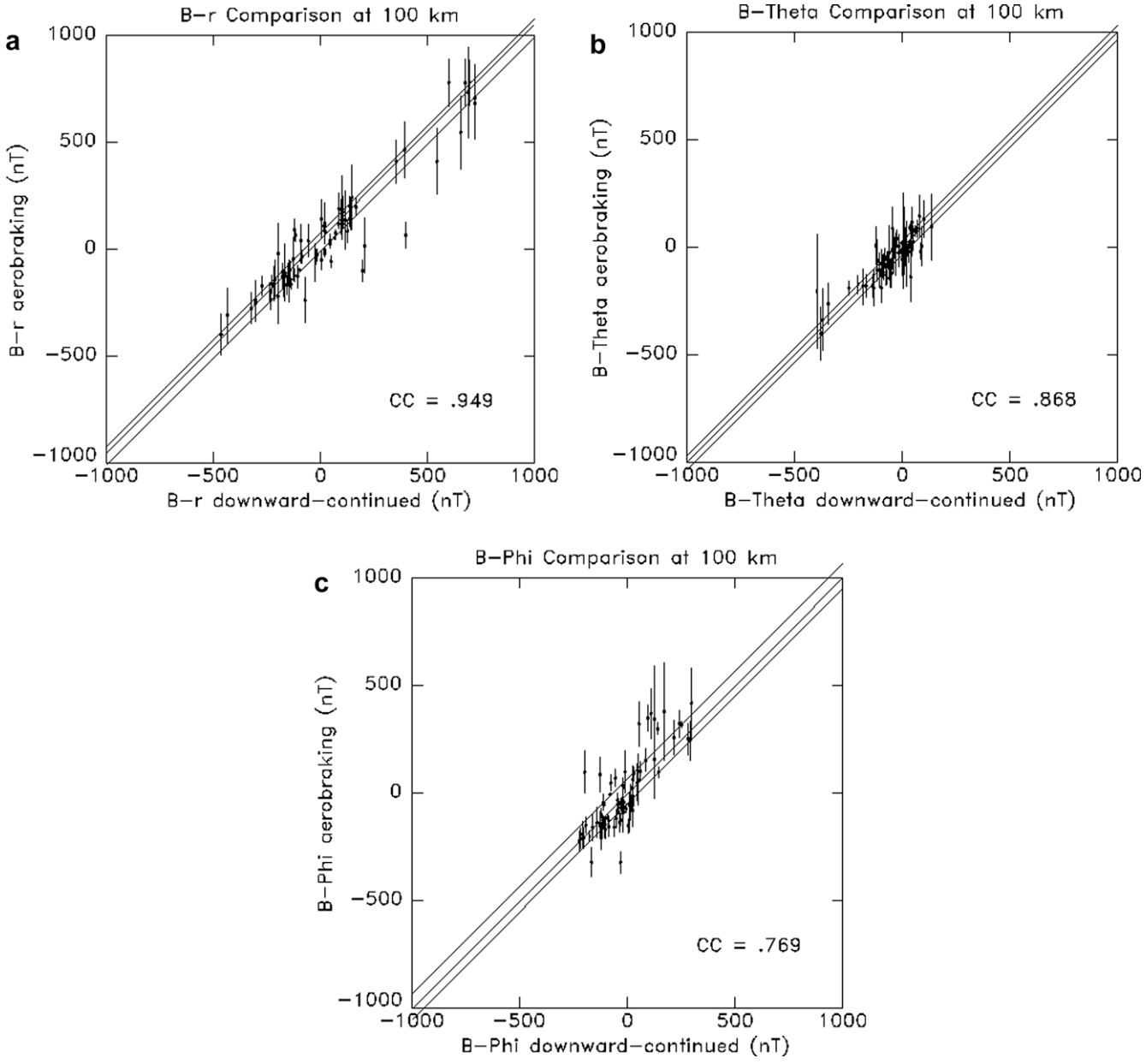

Fig. 2. (a) Downward-continued value of mapping-level data, B_r, at 100 km compared at 90 selected grid locations with measurements at aerobraking elevations along with their associated standard deviation, σ. Aerobraking measurements from elevations 80–190 km, from data in 10 km altitude bins. Best fitting line shown with one standard deviation. (b) Comparison for B_θ, as in (a). (c) Comparison for B_Φ, as in (a).

quantitatively confirms our earlier visual assessment that the downward continued field closely matched the low level measurements. Both the locations of strong crustal magnetic field and the magnitudes of the aerobraking and downward-continued fields agree. Within these bins there was very good agreement with the extrapolated field. For this particular area – the region with the most strongly magnetized crust – little additional information appears to be contained in the aerobraking data set. However, this does not preclude the possibility that for other regions, ones with weak crustal field, that low-altitude data may be useful.

3. Models, sources and deconvolution

Next we use the vertical components of the magnetic field to find sources at a selected depth by means of a deconvolution and then drop all source values below a chosen threshold. The vertical component of the Fourier transform of the magnetic field is directly related to the transform of the scalar potential (Eq. (1), Jurdy and Stefanick, 2004). And from the derivatives of that scalar potential the horizontal components of the field can be obtained. (The units of the scalar potential are those of the field multiplied by one linear dimension.) The resulting isolated sources are used to construct a model field which can be compared with the original field for goodness of fit. In our earlier paper we selected centers by visual inspection, and then found depths and source magnitudes by fitting vertical dipoles that matched the scalar potential field near the center. The results were subjective, and the model fields looked artificial. Here we utilize deconvolution for a more objective determination of the magnetic source which can be viewed as vertical dipoles.

The deconvolution is performed by means of a transfer function (Kanasewich, 1981, p. 80). The Fourier transform of the source field will be the Fourier transform of the vertical component of the magnetic field multiplied by the transfer function. The transfer function is found by dividing the Fourier transform of a point source at the central grid point by the Fourier transform of the vertical component of the magnetic field of a magnetic source centered at the same central grid point and a chosen depth (e.g. 100 km).

For example, Fig. 3a shows the vertical component of the magnetic field, B_z, extrapolated down to 100 km and Fig. 3b shows the modeled magnetic field. The model field accounts for about 80% of the total variance, with a correlation coefficient 0.89. Fig. 3c shows the sources used to construct the model. The values range from −400 to −200 nT and from +200 to +400, i.e. values from −200 to +200 have been eliminated. Choosing the threshold at one-half the maximum values is arbitrary; for a Gaussian distribution the half-height approximately corresponds to two standard deviations. Here, the grid extends in latitude from 0° to −80° at the center latitude of 40°S. On the western border, geographical coordinates range from latitude 60°S, longitude 94° on the south to latitude 7°N, longitude 150° at the north. Similarly, the eastern boundary extends from 60°S, 266° to 7°N, 210°. These coordinates result from overlaying a Cartesian grid upon the southern hemisphere centered at 40°S, 180°.

Next we show the corresponding extrapolation for the field as a mathematical demonstration of the behavior of the noise. As we extrapolate downward from 400 km to the surface and then below using Laplace's equation, the minimum and maximum values of the field increase rapidly. Plotting their reciprocals against the altitude (Fig. 4), we see that the fields cannot be extrapolated far below the surface. Also, this again reveals a systematic difference in the behavior of positive (solid circles) and negative sources (open circles) with downward extrapolation. Although at 400 km mapping level the maximums of positive and negative sources are equivalent, they diverge with lower elevations. (By "positive" we mean those sources with the equivalent dipole directed outward.)

Spectral components increase exponentially with wavenumber with downward continuation. Since the signal components concentrate at low wavenumbers whereas the noise has a very broad spectrum, the extrapolated noise grows rapidly at high wavenumbers and the spectrum must be truncated, at wavenumber 25–30 as discussed earlier. With depth, the negative polarity minimum approaches infinity at $\gtrsim$ 100 km (for display inverses are plotted), suggesting weaker signal and greater noise contribution. For extrapolation with either the linear or parabolic fit, the positive polarity would not reach infinity until very much deeper. We believe that this documents a fundamental difference between normal and reversed polarities in magnetization in this quadrant of the Martian Southern Hemisphere.

Using the vertical component, we have constructed the field for the region with the strongest magnetization. We have used the field to extrapolate to the surface, and then by means of a deconvolution obtained the sources. The sources were used to model the field, yielding very good results in terms of fit and appearance.

4. Interpretation of magnetization

The southern hemisphere region from longitude 150 to 210, nearly an octant of Mars' surface, contains the most extensive and strong magnetization. Our analysis has shown the field over this large region can be modeled with relatively few sources. However, an apparent dichotomy exists based on the polarity of model sources. Positive sources are stronger, and they also outnumber negative ones; the negative sources contain greater noise. The magnetic sources used to model the field do not appear to be randomly arranged, nor suggest alternating bands. In this section we consider the tectonic and geological setting of the magnetic sources. Of interest is any association of sources to craters and ringed basins and the system of Tharsis-related faults. The goal is an improved understanding of the process and timing of magnetization and demagnetization.

4.1. Surface association of magnetization

Highland terrain materials with some younger northern channel materials and southern polar deposits cover the southern hemisphere region analyzed (Greeley and Guest, 1998; Scott and Tanaka, 1998; Tanaka and Scott, 1998). Of particular interest are the location of ancient impacts that no longer retain the topographic signature of fresh craters, but instead have been identified by concentric basins and outflow channels (Schultz et al., 1982). The multi-ringed basins from north to south in this region are Mangala, Al Qahira, S. of Hesphaestus Fossae, and Sirenum (locations and ring diameters in Table 2, Schultz et al., 1982). The magnetic field, extrapolated to the planet's surface from satellite level can be compared with surface features (Fig. 3).

Earth's impacts offer analogs for Mars. Small craters, such as the 24-km Houghton feature in Canada (Parnell et al., 2005), did not reach very high temperatures during impact, based on indisputable evidence from the alteration of organic material. However, larger impacts would cause higher temperatures and pressures. Chicxulub, just 100 km-sized, has been documented by seismic reflection data as a multi-ringed basin, with deformation to the base of the crust (Morgan and Warner, 1999). Mars' multi-ring basins significantly exceed this size.

An impact in the presence of a magnetic field would result in magnetization. The presence of water would facilitate magnetization by creating nanophases in the presence of an existing planetary field. Schultz et al. (1982) argue for hydrothermal activity

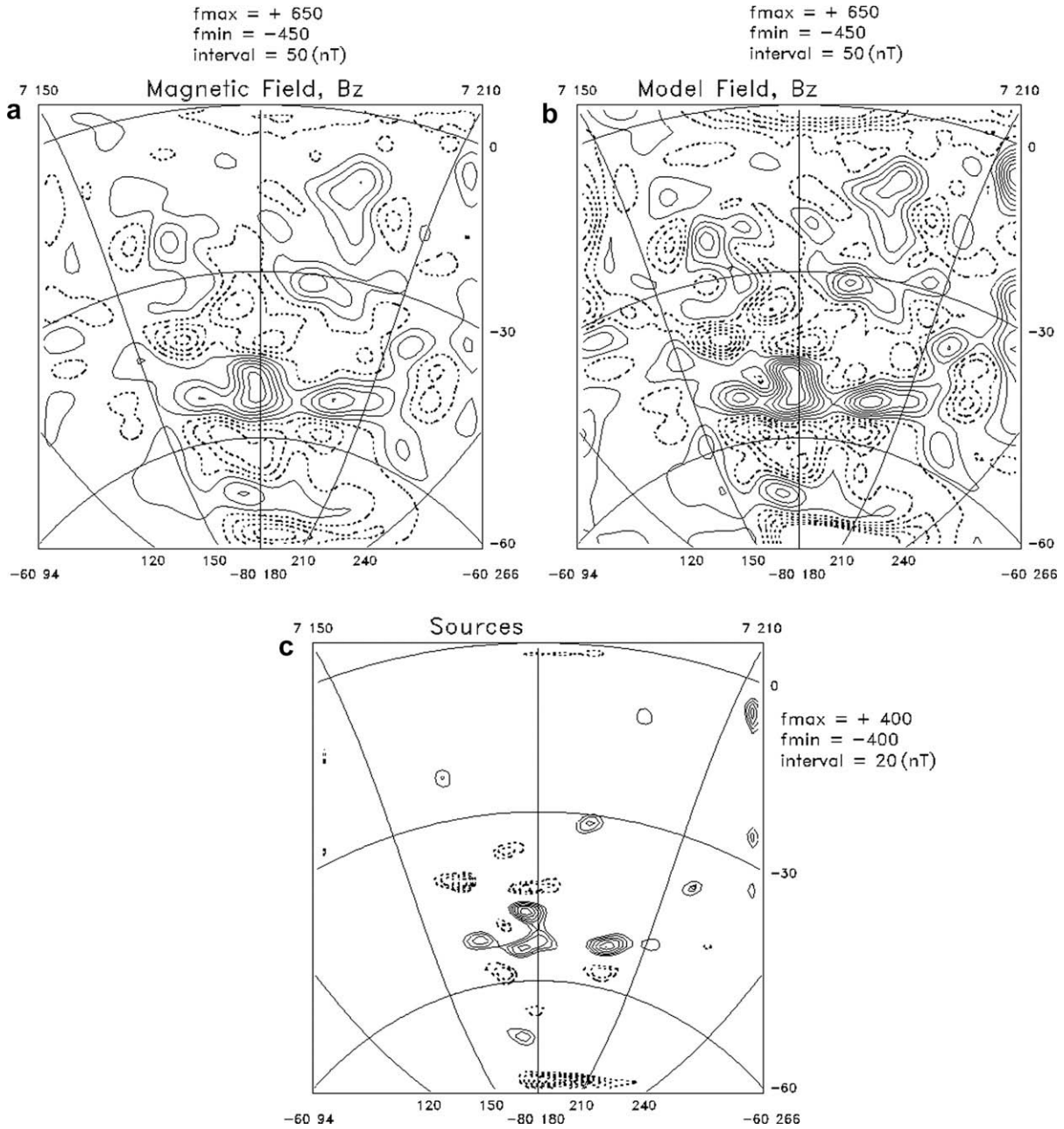

Fig. 3. (a) The magnetic field, B_z, extrapolated downward to an elevation of 100 km above the surface of Mars. Solid lines contour positive values and zero; dashed lines used for negative values. Map centered at 40°S, 180°W, extending 40° in each direction. Latitude and longitude lines shown for reference with the geographical coordinates of the corners given. (b) Model for the magnetic field at 100 km. (c) Sources for the modeled magnetic field (b); for clarity field filtered to eliminate amplitudes less than half the maximums.

associated with impacts which in the presence of a magnetic field could account for the locations of strong magnetization here. However, igneous activity that concentrates along the rings stands out as key. Therefore, it seems reasonable that these early impacts on Mars would eradicate any earlier magnetization and then could cause remagnetization by igneous activity and also possibly by the mobilization of water – if a planetary magnetic field existed at the time of impact.

In general, impact craters larger than 300 km disrupt magnetization (Acuna et al., 1999) even out to several radii, however, in the southern hemisphere modification of the surface magnetization is not obvious surrounding the ringed basins. Indeed, some of the strongest field lies immediately adjacent to the rings of the ancient impacts. In particular, for the southernmost structure with the Sirenum basin, the scalar potential contour lines appear to curve around the outermost 1000 km ring as identified by Schultz et al. (1982). As we previously noted for scalar potential, the warping of the contour lines around the Sirenum basin circles becomes most evident with the downward continuation of the field to near surface level (Fig. 4a, Jurdy and Stefanick, 2004). Possibly, then, in the southern hemisphere remagnetization immediately followed the early impacts causing the large basins like Sirenum. The interiors of these basins are weakly magnetized (Fig. 5a), but for the four concentric basins shown, locations of strong magnetization coincide with outer rings or are located adjacent. These ancient basins no longer retain the topographic signature of more recent impact crater; rather, identification has been based upon stream directions, capture, and structural control

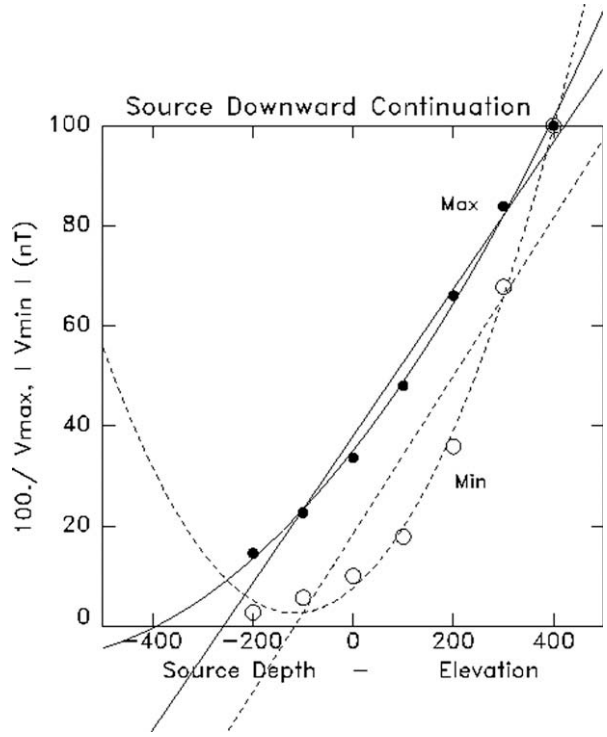

Fig. 4. Reciprocals of maximums and minimums of sources in model shown as a function of altitude and depth of extrapolation. Linear and parabolic fits are made for maximums of the positives (solid circles) and for minimums of the negatives (open circles). The negative polarity minimum approaches infinity at $\gtrsim 100$ km, suggesting weaker signal and greater noise contribution for the negative polarity than for the positive polarity which would only reach infinity at very much deeper depths.

(Schultz, personal communication). For comparison, a set of craters based on MOLA topography (Frey, 2008) is shown in Fig. 5b.

In the southern hemisphere region, there appears to be an association of magnetic sources with ringed basins which dominate the area. In the next section we statistically evaluate the likelihood of this association.

4.1.1. Test for association of magnetic sources with impacts

A number of the magnetic sources appear to lie near, but just outside, of the multi-ringed basins. We test the association for the 18 sources in this region to quantify their proximity or avoidance of ringed basins and then assign a probability for the observed occurrence. Here we present an argument using χ^2 statistics (Fisher, 1973) to assess the likelihood of the observed distribution. The analysis for the area is repeated for craters based on MOLA topography (Frey, 2008).

We create three fictitious regions: (1) within basins, (2) near basins, and (3) away from basins, defined in some reasonable way. Each of these regions has an area; the sum of these areas equals the area of the entire square, nearly an octant of Mars' surface. For a uniform distribution, the fraction of the fictional area times the total number of sources gives the expected number of sources in each region. The χ^2 statistic measures the goodness of fit:

$$\chi^2 = \sum \frac{(\bar{n}_m - n_m)^2}{n_m} \tag{6}$$

where $\bar{n}_m$ is the observed count for each of m regions, three in this case, and n_m, the expected count based on relative area.

Areas of each of the three regions are estimated. Employing a $5^\circ \times 5^\circ$ grid with a total of 256 boxes, we count the number encompassed within basins, near basins, and away from basins. Boxes inside basin rings are regarded as "within"; here we arbitrarily define "near" as the region between the outer basin ring out to three radii or a maximum of 3000 km. And those remaining boxes beyond the three radii limit then count as "away from basins". We find: 33 boxes within, 112.5 near, and 110.5 away from basins, corresponding to fractional areas of .129, .439, and .432, respectively. (The half

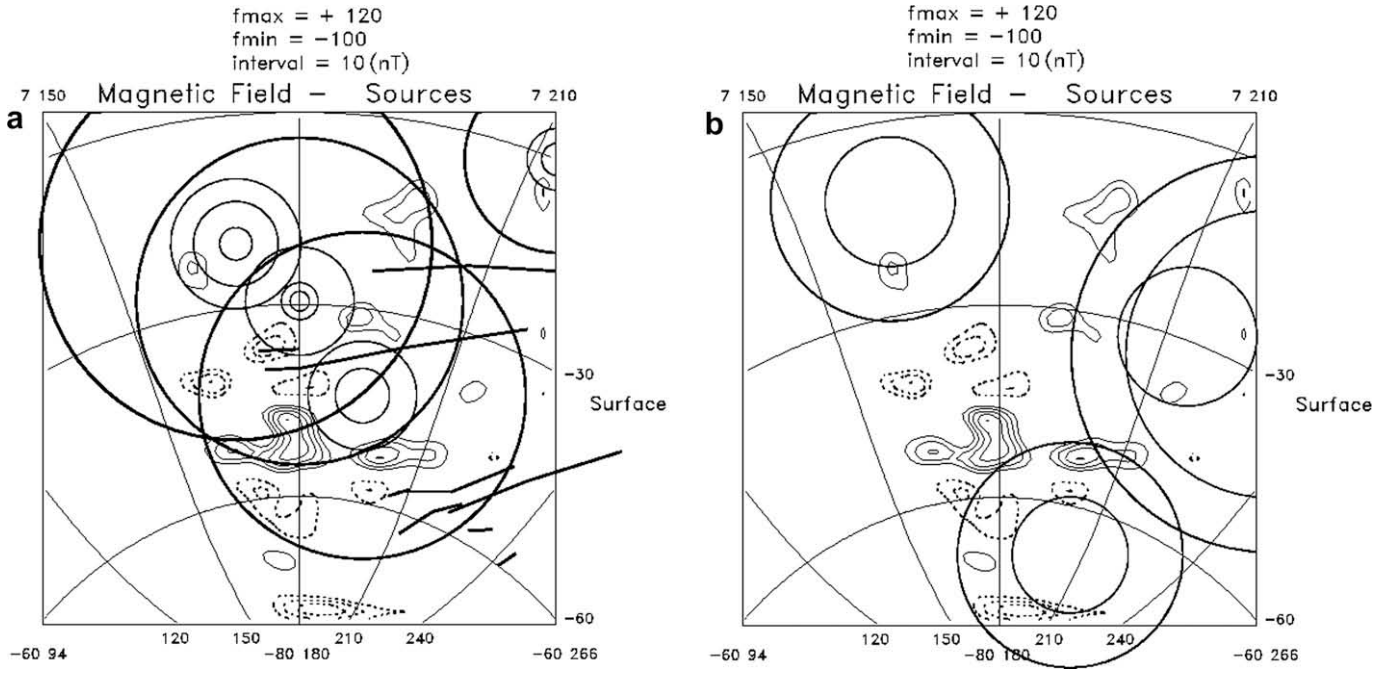

Fig. 5. (a) Sources for magnetic field vertical component, B_z at Mars' surface. Shown are four sets of concentric circles, multi-ringed basins, sites of ancient impacts, from north to south: Mangala, Al Qahira, S. of Hesphaestus Fossae, and Sirenum [locations and ring diameters as mapped by Schultz et al. (1982)]. Faults related to Tharsis-uplift shown as heavy lines [USGS Geological Maps]. Map projection as in Fig. 3. (b) Craters based on MOLA topography, from north to south: Zephyria, Daedalia, SW Daedalia, and Sirenum, locations and diameters from Frey (2008, Table 1). Outermost circle shown 1000 km beyond each crater's diameter to arbitrarily define "near". Sources as in (a).

units come from averaging counts, done twice: once vertically, then horizontally.)

The distribution of magnetic sources is assessed by assigning each to the one of the three basin regions: within, near, away. The fuzziness of the sources results from, at least in part, the deconvolution being only approximate. An exact deconvolution would require all wavenumbers being used, but we have zeroed out all high wavenumbers to limit noise, as discussed earlier. The observed counts: two sources within basins, 14 nearby, and two away from basins. However, for a uniform distribution of 18 sources with the relative areas determined, we would expect to find 2.32 sources within the basins, 7.90 near basins and the remaining 7.78 sources in the region defined as away from the basins. For this case χ^2 can be computed, summing within-, near- and away from-basin regions:

$$\chi^2 = \frac{(2-2.32)^2}{2.32} + \frac{(14-7.90)^2}{7.90} + \frac{(2-7.78)^2}{7.78} = 9.05 \quad (7)$$

Here, the χ^2 value is calculated as ~9.0. The χ^2 values for two degrees of freedom generally lie in the range 0.5–3.0; values greater than 6.0 will occur only 5% of the time, a value of 7.8 only 2% of the time, and 9.2 only 1% of the time. Therefore the χ^2 analysis (7) shows the observed distribution of sources and ringed basins in the southern hemisphere area near 40°S, 180° to be a low-probability occurrence. A slight reinterpretation of source locations resulting in 13 nearby and three outside would lower the χ^2 value to 6.3, having a probability of ~5%.

For comparison, we next repeat the statistical analysis for magnetic sources with another impact scenario. Frey's (2008) recent global assessment of large craters for Mars has been correlated with magnetization by Lillis et al. (2008) to establish the duration of Mars' global magnetic field. Four craters (locations and sizes given in Table 1, Frey, 2008) fall within 40° of latitude 40°S, 180°W: Zephyria, Daedalia, SW Daedalia, and Sirenum, from north to south. (This catalogue positions Sirenum at 67.4°S, 154.7°W, whereas previously a feature at 43.5°S, 166.5°W, about the same size, was given the same name.) We repeat the χ^2 analysis. Counting 5° boxes for this alternative set of craters we find 51 boxes lie within the craters, 82 near and the remaining 123 outside, corresponding to fractional areas of .199, .320, and .481, respectively. (Here we arbitrarily define "near" as within 1000 km of each crater's outer diameter.) For the 18 sources, based on these fractional areas, 3.6 sources would be expected within craters, 5.8 nearby and 8.6 away from craters; however, counting sources we find only one source lies within a crater, 13 nearby and four away from craters. This corresponds to χ^2 value of 9.34, an unusual association, occurring only ~ 1% of the time. This statistical analysis in the Martian Southern Hemisphere strongly suggests that magnetic sources are associated with ringed basins as the sites of ancient impacts as identified from geology (Schultz et al., 1982). In addition, re-analysis for an alternative distribution of Mars' largest craters – ones identified by Frey (2008) from MOLA topography – with the magnetic sources in this region, finds this alternative arrangement of basins and magnetic sources also unlikely to be random. However, because of the small number of points – 18 magnetic sources here – the results cannot be regarded as conclusive. A more refined description of inside-, near- and away-from basins would not remove the small number problem. Here we have developed and tested a hypothesis: that the strongest magnetic sources are located adjacent to, but not actually within, very large impacts or ringed basins. This can be tested in other regions.

A system of faults extends through the area. Most apparent in the western region (Scott and Tanaka, 1998), the faults also extend beyond 180° and die out to the east (Greeley and Guest, 1998). The model sources for B_z (Fig. 5) hint at a curious relation to the faults: often a fault trace separates two locations of strong magnetization. This – if confirmed – might indicate that the uplift of Tharsis and related faulting disrupted crust that had already been magnetized. We do not attempt a statistical test for the association, with the limited number of magnetic sources and faults even more restricted than craters. However, the hypothesis merits further examination in other regions where it can be better tested and assessed. Possibly, the timing of the faults caused by the uplift of Tharsis could further bracket the duration of the Martian magnetic field.

5. Discussion

All of the ringed basins in the southern hemisphere octant centered on 40°S, 180° have magnetic sources immediately adjacent. The impact process in the presence of an active magnetic field could cause local magnetization. Igneous activity concentrating along the rings would record the magnetic field at the time of impact. If water were present, hydrothermal activity caused by the impacts could also contribute to magnetization of the ringed basins. Some large craters such as Argyre and Hellas have experienced demagnetization, but Mitchell et al. (2007) show Utopia as featuring a ring of "enhanced values" of the crustal magnetic field at an altitude of 170 km, B_{170}. So either Utopia demagnetized an already magnetized region, leaving patches, or the sources represent magnetization of Utopia's inner ring at impact. The latter would, they note, establish the existence of the Martian magnetic field at the time of Utopia's impact. On the basis of crater density Utopia predates Hellas and Argyre, both lacking internal magnetization (Mitchell et al., 2007).

From numerous studies (e.g. Arkani-Hamed, 2001a; Hood et al., 2005), it appears probable that different regions on Mars were magnetized relative to different past locations of the magnetic pole and therefore of the spin axis. However, each determination requires assumptions, and the resulting paleopole locations scatter considerably over the surface. Magnetization of ringed basins at time of impact could offer an independent approach for the determination of magnetic pole locations. If a region were located near Mars' magnetic north pole at the time of magnetization this would account for the numerous vertical dipoles causing the corresponding excess of positive sources in the southern hemisphere near latitude 40°S, longitude 180°. For the path proposed by Schultz and Lutz (1988), the pole wanders through this region during the Middle Noachian to the Early Hesperian. In this scenario for Martian true polar wander, only the final push about 3 billion years ago brought the pole to its current location (P. Schultz, personal communication, 2004).

Confirmation of the cause and timing of magnetization associated with ringed basins requires further examination, particularly the downward continuation of the field to the surface. Accurate positioning of magnetic sources at Mars' surface and possibly below, along with the incorporation of MOLA topographic data could clarify the geometric relation of magnetization to the igneous activity of the rings. Analysis of an isolated, but similarly-aged basin in another region would be most informative. If the magnetization resulted from the impacts, this could further constrain the extent of the magnetic field on Mars. The south polar area holds promise for further modeling.

6. Conclusions

We studied the strongly magnetized region in the southern hemisphere within 40° of the point at 40°S, 180°W, covering nearly an octant of Mars' surface. Using a rotated Cartesian coordinate system allowed application of ordinary two-dimensional Fourier

analysis for downward continuation. Comparison of downward-continued, mapping level field with aerobraking measurements made at 100 km for bins having angular deviation within ±30° yields a 95% correlation for the vertical component, B_r. One explanation for this agreement would be that the lower-level at ~100 km does not contain significant magnetic signal at lower wavelengths than that measured in the mapping field ~400 km. This would have important consequences for the origin and analysis of Mars' magnetic field and requires further analysis. The magnetic field components were used to model the sources for the field. A small number of discrete sources, ~10–12, more positive ones than negative, can model the field over this large area. However, in a mathematical test of noise, with downward continuation the negative sources more quickly approach infinity, suggesting weaker inherent signal and a greater contribution of noise. This may signify a fundamental difference here between normal and reversed polarity for Mars' magnetization.

Models for the field in this southern hemisphere region neither require magnetic stripes with reversals, nor rule out the possibility either. Statistical analysis supports the observation that many of the strongest magnetic sources appear to lie near to the outer rings of ancient impacts. The ringed basins, Mangala, Al Qahira, S. of Hesphaestus Fossae, and Sirenum, all have weakly magnetized interiors, with magnetic sources situated near their outer rings. These no longer retain the topographic signature of more recent impact crater and were identified from geological constraints. Statistical analysis was repeated for an alternative set of impact sites, craters identified from their topographic signature. For both of these alternatives we test the likelihood of the association by comparing the observed sources found within and near basins with random distribution; the observed distributions were found to be a low-probability occurrence for both of the basin scenarios. Impacts in the presence of a magnetic field – and perhaps water – may be responsible for the observed magnetization around ringed basins. In this southern hemisphere region there are only a few large impacts and about a dozen magnetic sources. Therefore, the hypothesis that the strongest magnetic sources are positioned adjacent to, but not actually within, very large impacts or ringed basins needs to be tested elsewhere. If a geometric relation between the magnetization and impact rings could be established, this might offer an independent approach for determining Martian paleomagnetic poles. If confirmed, then the magnetization may be contemporaneous with the impacts; this would provide an additional constraint on the duration of Mars' magnetic field.

Acknowledgments

The MGS mapping dataset, binned by latitudes and longitudes, was the basis of our study. This dataset was generously made available to the scientific community by Connerney and coauthors; we thank Jack Connerney for discussions on noise and downward continuation. We are grateful to Pete Schultz for sharing his insights on impacts and for his continued encouragement. Finally, we thank Editor Jim Bell for his forbearance. We are grateful for funding from Mars Data Analysis Program, Grant #NAG5-12157 that supported this research.

References

Acuna, M.H., and 13 colleagues, 1999. Global distribution of crustal magnetization discovered by the Mars Global Surveyor MAG/ER experiment. Science 284, 790–793.

Arkani-Hamed, J., 2001a. Paleomagnetic pole positions and pole reversals of Mars. Geophys. Res. Lett. 17, 3409–3412.

Arkani-Hamed, J., 2001b. A 50-degree spherical harmonic model of the magnetic field of Mars. J. Geophys. Res. 106, 23197–23208.

Cain, J.C., Ferguson, B.B., Mozzoni, D., 2003. An $n = 90$ internal potential function of the martian crustal magnetic field. J. Geophys. Res., 108. doi:10.1029/2000JE001487.

Carslaw, H.S., 1930. Introduction to the Theory of Fourier Series and Integrals. Dover, New York.

Claerbout, J.F., 1976. Fundamentals of Geophysical Data Processing. McGraw-Hill, New York. 274pp.

Connerney, J.E.P., Acuna, M.H., Wasilewski, P.J., Ness, N.F., Reme, H., Mazelle, C., Vignes, D., Lin, R.P., Mitchell, D.L., Cloutier, P.A., 1999. Magnetic lineations in the ancient crust of Mars. Science 284, 794–798.

Connerney, J.E.P., Acuna, M.H., Wasilewski, P.J., Kletetschka, G., Ness, N.F., Reme, H., Lin, R.P., Mitchell, D.L., 2001. The global magnetic field of Mars and implications for crustal evolution. Geophys. Res. Lett. 28, 4015–4018.

Connerney, J.E.P., Acuna, M.H., Ness, N.F., Mitchell, D.L., Lin, R.P., Reme, H., 2005. Tectonic implications of Mars crustal magnetism. Proc. Natl. Acad. Sci. USA 102, 14970–14975.

Dahlquist, G., Bjorck, A., 1997. Numerical Methods. Prentice-Hall, Englewood Cliffs, NJ. 573pp.

Espley, J.R., Connerney, J.E.P., Jurdy, D.M., Acuna, M.H., 2007. Downward continuation of the martian magnetic field. Lunar Planet. Sci. XXXVIII (abstract).

Fisher, R.A., 1973. Statistical Methods for Research Workers. Hafner, New York. 362pp.

Frey, H.V., 2008. Ages of very large impact basins on Mars: Implications for the late heavy bombardment in the inner Solar System. Geophys. Res. Lett., 35. doi:10.1029/2008GL033515.

Greeley, R., Guest, J.E., 1998. Geologic map of the eastern equatorial region of Mars. USGS, Geological Investigations Series Map I, I-1802-B.

Hood, L.L., Young, C.N., Richmond, N.C., Harrison, K.P., 2005. Modeling of major martian magnetic anomalies: Further evidence for polar reorientations during the Noachian. Icarus 177, 144–173.

Jurdy, D.M., Stefanick, M., 2003. Mars magnetic data: The impact of noise on the vertical extrapolation of fields and methods of suppression (abstract). Lunar Planet. Sci. XXXIII.

Jurdy, D.M., Stefanick, M., 2004. Vertical extrapolation of Mars magnetic potentials. J. Geophys. Res., doi:10.1029/2004JE002277.

Kanasewich, E.R., 1981. Time Sequence Analysis in Geophysics. University of Alberta Press, Alberta, Canada. 480pp.

Klein, F., 1925. Arithmetic, Algebra, Analysis, third ed., Translated by E.R. Hedrick and C.A. Noble. Dover, New York.

Lillis, R.J., Frey, H.V., Manga, M., 2008. Rapid decrease in martian crustal magnetization in the Noachian era: Implications for the dynamo and climate of early Mars. Geophys. Res. Lett. 35. doi:10.1029/2008GL034338.

Mitchell, D.L., Lillis, R., Lin, P., Connerney, J., Acuna, M., 2007. A global map of Mars' crustal magnetic field based on electron reflectometry. J. Geophys. Res. 112 (E1), E01002. doi:10.1029/2005JE002564.

Morgan, J., Warner, M., 1999. Chicxulub: The third dimension of a multi-ring impact basin. Geology 27, 407–410.

Nagy, A.F., and 14 colleagues, 2004. The plasma environment of Mars. Space Sci. Rev. 111, 33–114.

Nimmo, F., Gilmore, M.S., 2001. Comments on the depth of magnetized crust on Mars from impact craters. J. Geophys. Res. 106, 11315–11323.

Parnell, J., Osinski, G.R., Lee, P., Green, P.F., Baron, M.J., 2005. Thermal alteration of organic material in an impact crater and the duration of post-impact heating. Geology 33, 373–376.

Press, W.H., Teukolsky, S.A., Vetterling, W.T., Flannery, B.P., 1992. Numerical Recipes in FORTRAN. Cambridge University Press, New York. 818pp.

Rochette, P., Fillion, G., Ballou, R., Brunet, F., Ouladdiaf, B., Hood, L., 2003. High pressure magnetic transition in pyrrhotite and impact demagnetization on Mars. Geophys. Res. Lett. 30 (13), 1683. doi:10.1029/2003GL017359.

Schultz, P.H., Lutz, A.B., 1988. Polar wandering on Mars. Icarus 73, 91–141.

Schultz, P.H., Schultz, R.A., Rogers, J., 1982. The structure and evolution of ancient impact craters on Mars. J. Geophys. Res. 87, 9803–9820.

Scott, D.H., Tanaka, K.L., 1998. Geologic map of the western equatorial region of Mars. USGS, Geological Investigations Series.

Sleep, N.H., 1994. Martian plate tectonics. J. Geophys. Res. 99, 5639–5655.

Tanaka, K.L., Scott, D.H., 1998. Geologic map of the polar regions of Mars. USGS, Geological Investigations Series Map I, I-1802-C.